Supplement of Atmos. Chem. Phys., 18, 11793–11812, 2018
https://doi.org/10.5194/acp-18-11793-2018-supplement

Atmospheric Chemistry and Physics
Open Access

Supplement of

First long-term and near real-time measurement of trace elements in China's urban atmosphere: temporal variability, source apportionment and precipitation effect

Yunhua Chang et al.

Correspondence to: Yanlin Zhang (dryanlinzhang@outlook.com, zhangyanlin@nuist.edu.cn)

Table S1. Inter-comparison between ICP-MS and Xact for trace elements ("n" represents the number of paired samples).

Species	8 glass filters vs. Xact	all glass filters vs. Xact	8 cellulose filters vs. Xact	all cellulose filters vs. Xact	all 48 filters vs. Xact
K	y=1.06x+135 R^2=0.85 n=7	y=1.07x+72 R^2 = 0.87 n=21	y=1.03x+121 R^2=0.96 n=8	y=1.13x+131 R^2 = 0.91 n=25	y=1.08x+110 R^2 = 0.86 n=46
Cr	y=1.13x+0.51 R^2=0.92 n=3	y=1.77x-17 R^2=0.75 n=8	y=1.69x-3.9 R^2=0.65 n=6	y=1.92x-0.54 R^2=0.58 n=21	y=1.83x-0.48 R^2=0.49 n=29
Mn	y=0.87x-5.1 R^2=0.92 n=4	y=0.67x+12 R^2=0.52 n=18	y=0.85x-5.9 R^2=0.87 n=8	y=0.89x+9.5 R^2=0.66 n=25	y=0.79x+10.7 R^2=0.59 n=43
Fe	y=2.0x-257 R^2 =0.99 n=3	y=1.67x-97 R^2 = 0.95 n=10*	y=0.98x-21 R^2 =0.81 n=6	y=1.01x-22 R^2 = 0.82 n=20	y=1.03x+6.5 R^2 = 0.78 n=30*
Ni	y=1.62x-6.9 R^2=0.32 n=6	y=2.1x-13 R^2 =0.53 n=20	y=1.45x-6.1 R^2=0.54 n=7	y=1.09x+3.7 R^2 =0.55 n=23	y=1.32x+0.29 R^2 =0.49 n=43
Cu	y=1.97x -3.3 R^2=0.71 n=5	y=0.97x+5.6 R^2=0.40 n=19	y=0.89x+5.0 R^2=0.71 n=8	y=1.12+5.1 R^2=0.61 n=25	y=1.10+5.0 R^2=0.57 n=44
As	n=2	y=2.1x+0.19 R^2=0.48 n=5	y=2.2x-42 R^2=0.54 n=3	y=2.3x-19 R^2=0.49 n=4**	y=2.1x-16 R^2=0.36 n=9**
Cd	y=2.3x+1.04 R^2 = 0.90 n=7	y=1.99x+9.0 R^2=0.82 n=21	y=2.1x+5.0 R^2 = 0.80 n=8	y=1.97x+6.7 R^2=0.73 n=24	y=1.97x+8.1 R^2=0.76 n=45
Ba	y=2.9x-0.12 R^2=0.77 n=7	y=3.1x+0.04 R^2=0.78 n=21	y=2.5x-0.18 R^2=0.82 n=8	y=2.4x+0.29 R^2 =0.78 n=24	y=2.7x+0.20 R^2 =0.81 n=45
Au	y=0.97x+3.7 R^2=0.55 n=7	y=1.25x+2.0 R^2=0.72 n=21	y=1.18x+1.77 R^2=0.82 n=8	y=1.15x+1.50 R^2=0.84 n=23	y=1.17x+1.81 R^2=0.77 n=44
Pb	y=2.7x-0.12 R^2=0.68 n=7	y=2.1x+0.11 R^2=0.54 n=19	y=2.4x-0.10 R^2=0.85 n=8	y=1.74x+0.04 R^2=0.64 n=25	y=1.80x+0.09 R^2=0.59 n=44

Note: "*" indicates that an abnormal value of Fe (675 ng m^{-3}) collected by glass filter was excluded. "**" stands for the deletion of two abnormal values of As (63 and 78 ng m^{-3}) collected by cellulose filters.

Table S2. General information of the 12 precipitation events chosen in this study.

precipitation event ID	start	ending	accumulated rainfall amount (mm)
1	01-06 17:00	01-07 21:00	41
2	03-08 06:00	04-06 05:00	53
3	04-06 06:00	04-07 09:00	51
4	04-20 15:00	04-21 09:00	26
5	06-12 03:00	06-12 23:00	74
6	07-02 17:00	07-02 23:00	36
7	09-07 03:00	09-07 17:00	33
8	09-14 03:00	09-17 02:00	190
9	09-29 07:00	09-29 23:00	37
10	10-07 21:00	10-08 12:00	33
11	10-21 01:00	10-23 07:00	220
12	12-25 09:00	12-26 21:00	44

Section S1. PMF uncertainty analysis and factor number determination

In EPA PMF 5.0, bootstrapping (BS), displacement (DISP), and bootstrapping enhanced with DISP (BS-DISP) are used to estimate the results uncertainty. The methods were introduced in detail by Norris et al. (2014), Brown et al. (2015) and Paatero et al. (2014), and have been applied in source apportionment of $PM_{2.5}$ components (Liu et al., 2017; Wang et al., 2017).

BS analysis involves resampling from the original input data set, performing PMF analysis with resampled data set (bootstrapped solution), and the comparison of factor contributions between base-case and bootstrapped solutions. In this work, 100 BS runs in total were performed, and an *r* value of 0.8 was set to map the bootstrapped factor contributions with those of the base-case. The mapping of each BS factor contribution with the corresponding base-case factor contribution (5-factor solution) is shown in Table S3. All factors are mapped in more than 95 of the BS runs with five factors. If we select a factor number of six, one of the six factors is mapped in only 50 of the BS runs, and the other 5 factors are mapped in more than 95 of the BS runs. These results suggest a maximum factor number of five. Too many factors will split one source into multiple uninterpretable factors.

Table S3. Summary of error estimation diagnostics from BS.

BS Mapping (r ≥0.8)	traffic	shipping	nonferrous metal smelting	coal combustion	ferrous metal smelting	Unmapped
traffic	98	0	0	0	0	2
shipping	0	100	0	0	0	0
nonferrous metal smelting	0	0	100	0	0	0
coal combustion	0	0	0	100	0	0
ferrous metal smelting	0	0	0	0	97	3

DISP adjusts each species in the factor profile up and down one by one, and then performs PMF runs to obtain a change of Q (dQ, $Q_{\text{displaced run}} - Q_{\text{base run}}$) less than the selected maximum allowable dQ^{max} (4, 8, 15, 25). For each dQ^{max} value, DISP is conducted and the intervals (minimum and maximum source profile values) are summarized for each species in each factor. The DISP output is shown in Table S4. The error code is 0, meaning no error. The largest observed drop of Q during DISP is also 0. No factor swap occurs for the smallest dQ^{max}, suggesting a stable and robust

PMF solution, and there should be no rotational ambiguity.

Table S4. Summary of error estimation diagnostics from DISP.

Error Code:	0				
Largest Decrease in Q:	0				
%dQ:	0				
Swaps by Factor:	traffic	shipping	nonferrous metal smelting	coal combustion	ferrous metal smelting
dQ^{max}=4	0	0	0	0	0
dQ^{max}=8	0	0	0	0	0
dQ^{max}=15	0	0	0	0	0
dQ^{max}=25	0	0	0	0	0

BS-DISP is a combination of the BS and DISP methods, where displacement occurs in source profiles derived from each resampled data set. It estimates the errors associated with both random and rotational ambiguity. Due to the huge data set in this work, (7519 × 18), BS-DISP analysis is time consuming and not conducted.

Q/Q_{exp} was calculated for the PMF solutions with factor numbers from 3 to 10 (Fig. S1). When the factor number reaches 9, the Q/Q_{exp} will change less substantially (6.9%) than is the case when going from the 4- to the 5-factor solution (18.9%). However, a 5-factor solution was selected due to the most interpretable and stable results.

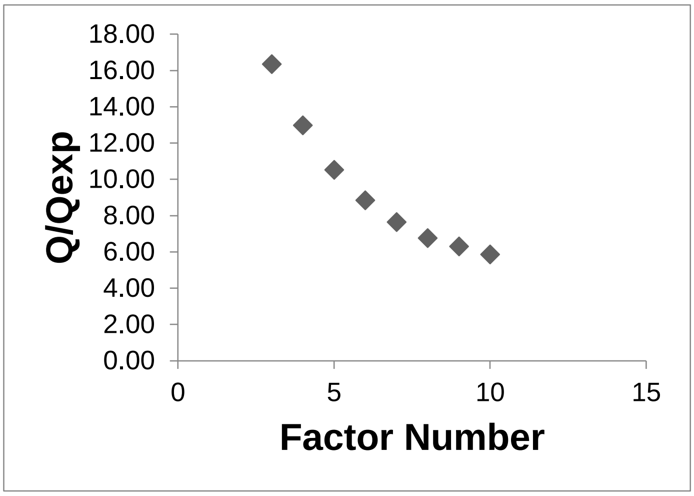

Figure S1. Change of Q/Q_{exp} value from 3-factor to 10-factor solution.

References

Brown, S.G., Eberly, S., Paatero, P., Norris, G.A., 2015. Methods for estimating uncertainty in PMF solutions: Examples with ambient air and water quality data and guidance on reporting PMF results. Science of The Total Environment 518-519,

626-635.
Liu, B., Wu, J., Zhang, J., Wang, L., Yang, J., Liang, D., Dai, Q., Bi, X., Feng, Y., Zhang, Y., Zhang, Q., 2017. Characterization and source apportionment of PM2.5 based on error estimation from EPA PMF 5.0 model at a medium city in China. Environmental Pollution 222, 10-22.
Norris, G., Duvall, R., Brown, S., Bai, S., 2014. EPA Positive Matrix Factorization (PMF) 5.0 Fundamentals and User Guide Prepared for the US Environmental Protection Agency Office of Research and Development. *Washington, DC*.
Paatero, P., Eberly, S., Brown, S., Norris, G., 2014. Methods for estimating uncertainty in factor analytic solutions. Atmospheric Measurement Techniques 7, 781-797.
Wang, Q., He, X., Huang, X.H., Griffith, S.M., Feng, Y., Zhang, T., Zhang, Q., Wu, D., Yu, J.Z., 2017. Impact of secondary organic aerosol tracers on tracer-based source apportionment of organic carbon and $PM_{2.5}$: a case study in the pearl river delta, China. ACS Earth and Space Chemistry 1, 562-571.

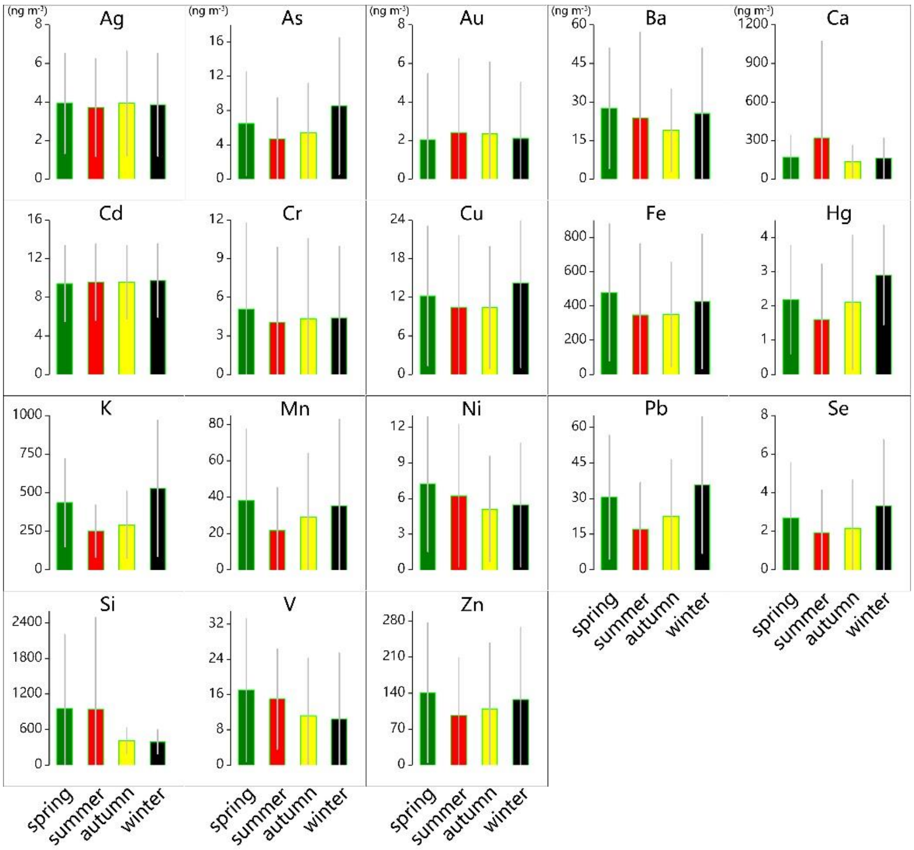

Figure S2. Seasonal variation of mass concentrations for 18 trace elements measured in Shanghai between March 2016 and February 2017. The gray line indicates one standard deviation. Four seasons in Shanghai were defined as follows: March-May as spring, June-August as summer, September- November as fall, and December and January-February as winter.

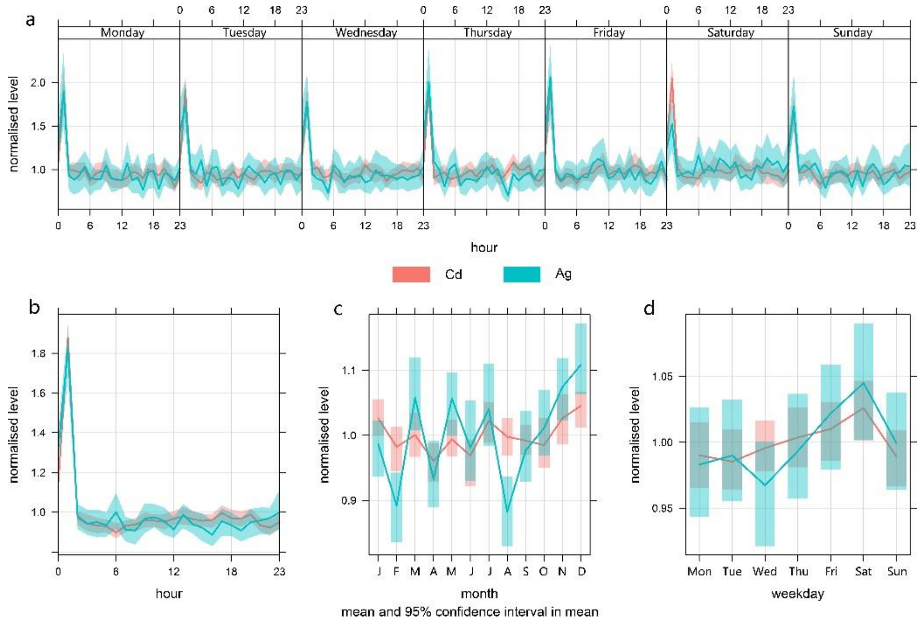

Figure S3. Weekly diurnal (**a**), diurnal (**b**), monthly (**c**), and weekly (**d**) variations of normalized Cd and Ag concentrations in Shanghai.

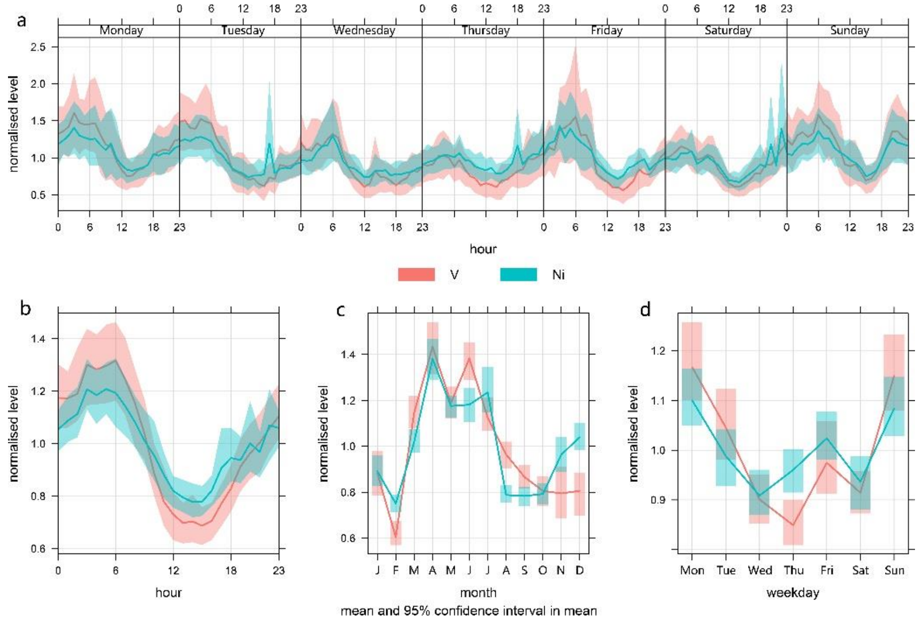

Figure S4. Weekly diurnal (**a**), diurnal (**b**), monthly (**c**), and weekly (**d**) variations of normalized V and Ni concentrations in Shanghai.

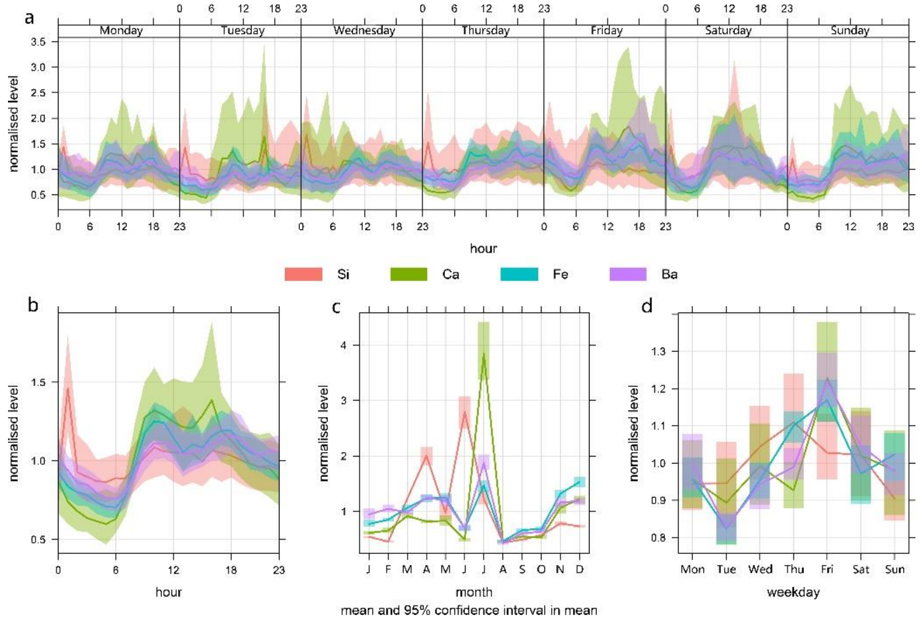

Figure S5. Weekly diurnal (**a**), diurnal (**b**), monthly (**c**), and weekly (**d**) variations of normalized Si, Ca, Fe, and Ba concentrations in Shanghai.

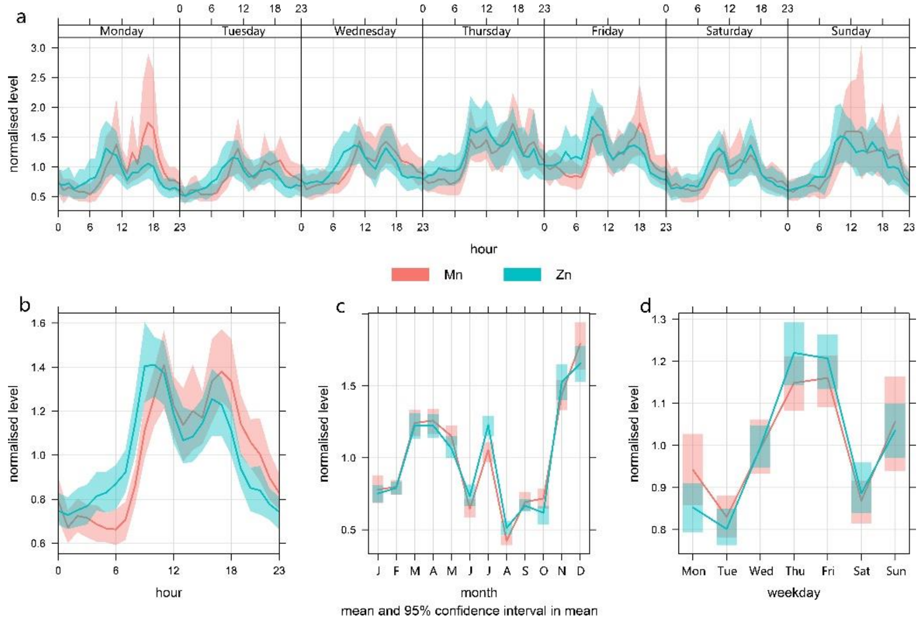

Figure S6. Weekly diurnal (**a**), diurnal (**b**), monthly (**c**), and weekly (**d**) variations of normalized Mn and Zn concentrations in Shanghai.

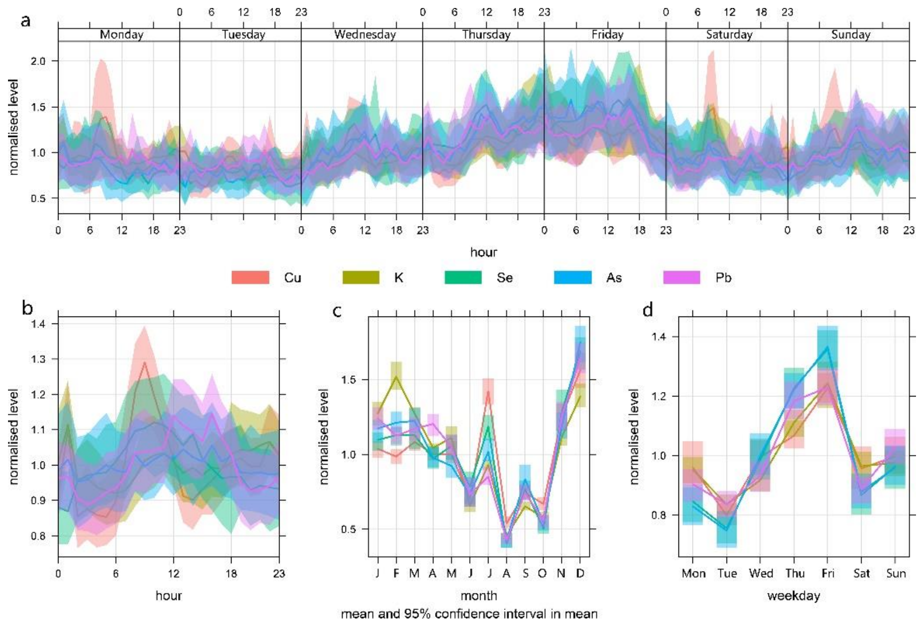

Figure S7. Weekly diurnal (**a**), diurnal (**b**), monthly (**c**), and weekly (**d**) variations of normalized Cu, K, Se, As, and Pb concentrations in Shanghai.

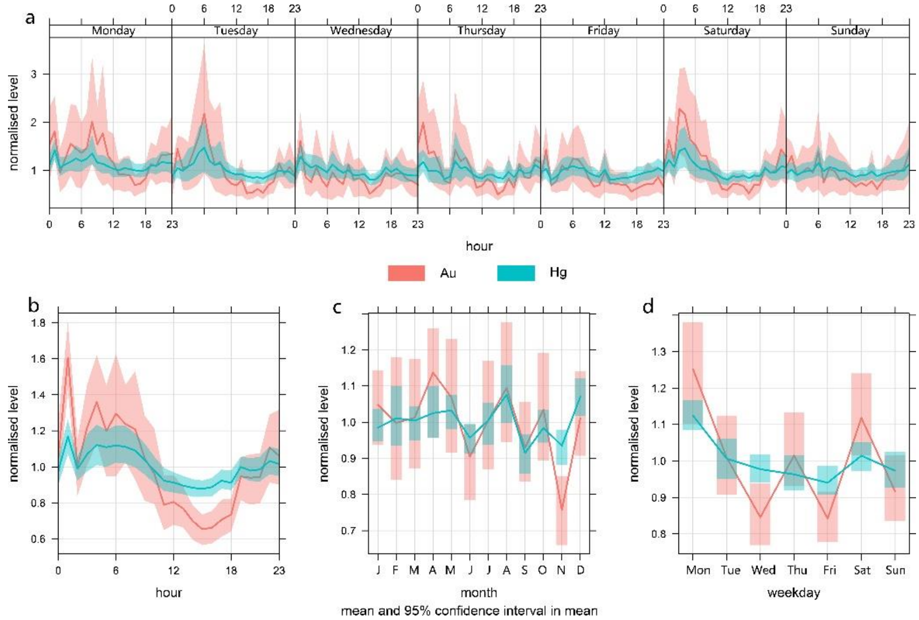

Figure S8. Weekly diurnal (**a**), diurnal (**b**), monthly (**c**), and weekly (**d**) variations of normalized Au and Hg concentrations in Shanghai.

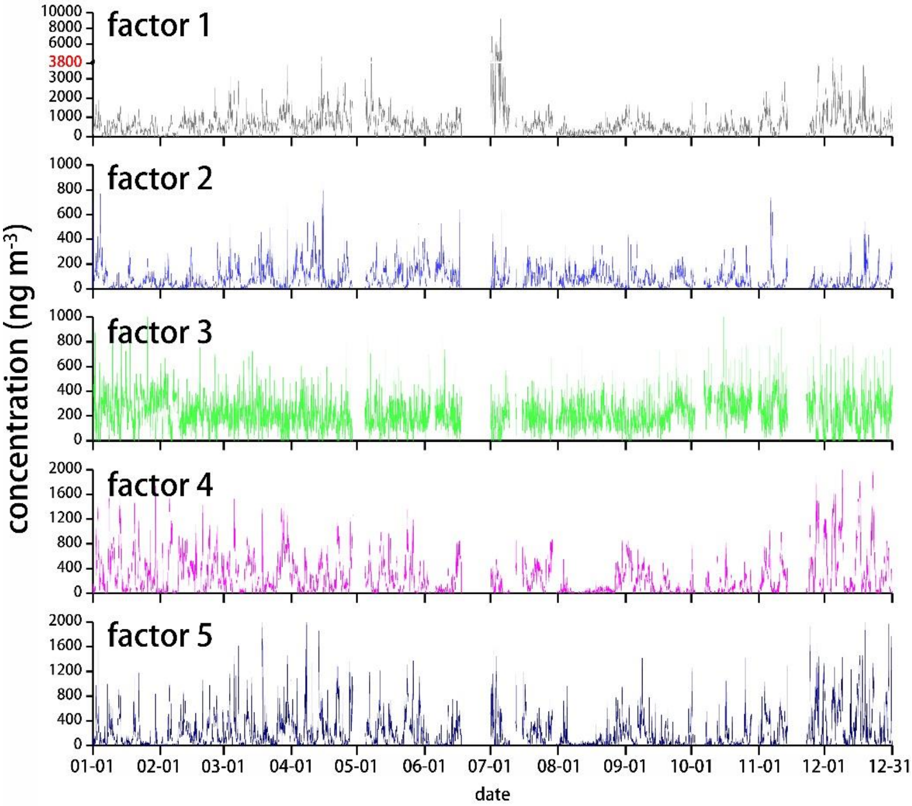

Figure S9. Time series plots of PMF-derived source contributions (in ng m^{-3}) for 18 trace elements in $PM_{2.5}$.

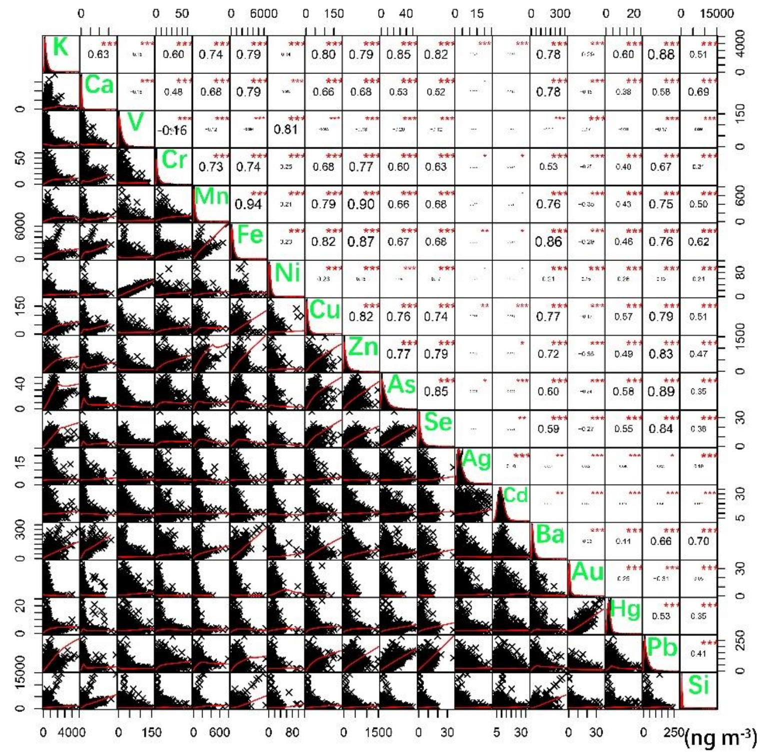

Figure S10. Spearman correlation matrix of 18 atmospheric elemental species in Shanghai between March 2016 and February 2017. The distribution of each species is shown on the diagonal. Below the diagonal, the bivariate scatter plots with a fitted line are displayed; above the diagonal, the value of the correlation plus the significance level as asterisks. Each significance level is associated to a symbol: *p*-values (0, 0.001, 0.01, 0.05, 0.1, 1) = symbols (“***”, “**”, “*”, “…”, “.. ”, “.”).

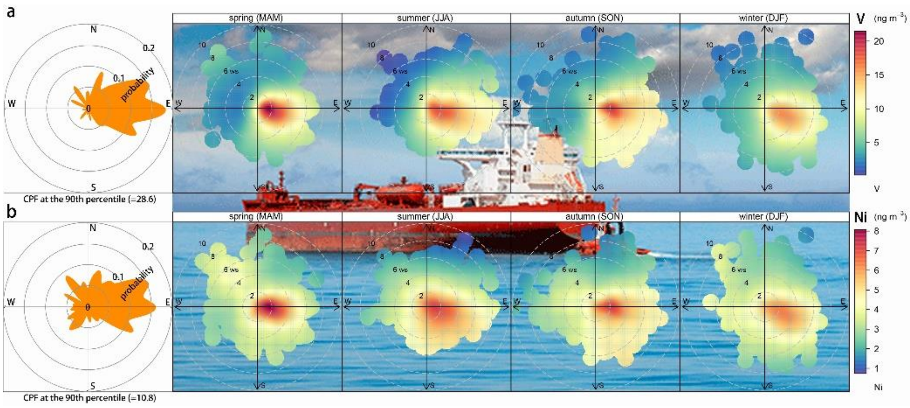

Figure S11. Conditional probability function analysis (left) and bivariate polar plots (right) of seasonal concentrations (ng m^{-3}) of V (**a**) and Ni (**b**) in Shanghai between March 2016 and February 2017. The center of each plot (centered at the sampling site) represents a wind speed of zero, which increases radially outward. The concentrations of V and Ni are shown by the color scale.

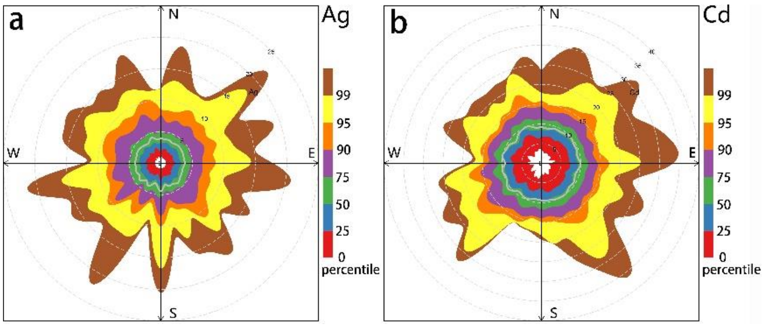

Figure S12. Percentile rose plot of Ag (**a**) and Cd (**b**) concentrations in Shanghai between March 2016 and February 2017. The percentile intervals are shaded and shown by wind direction.

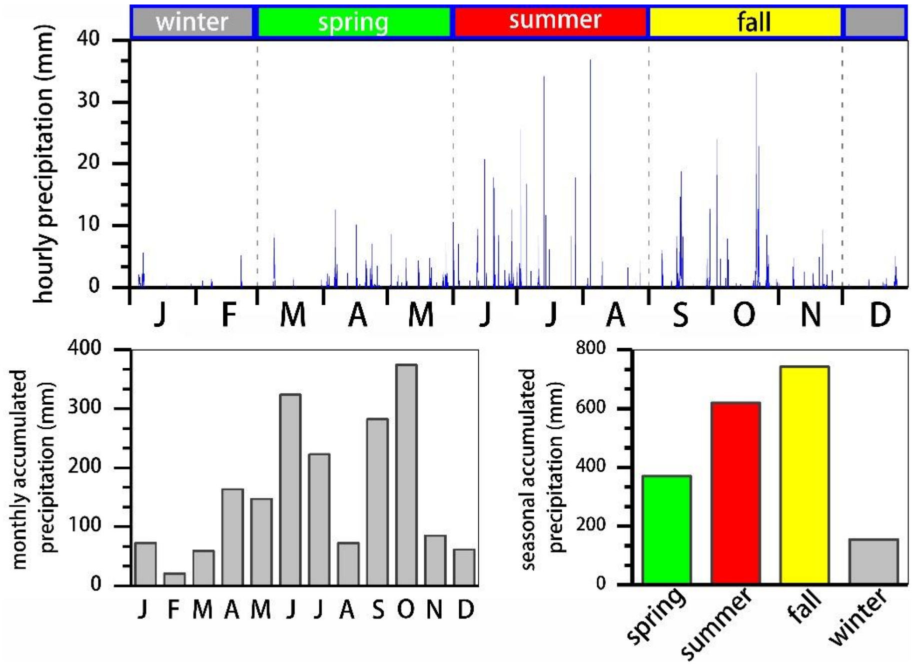

Figure S13. Distribution of precipitation events during the full year of measurements.

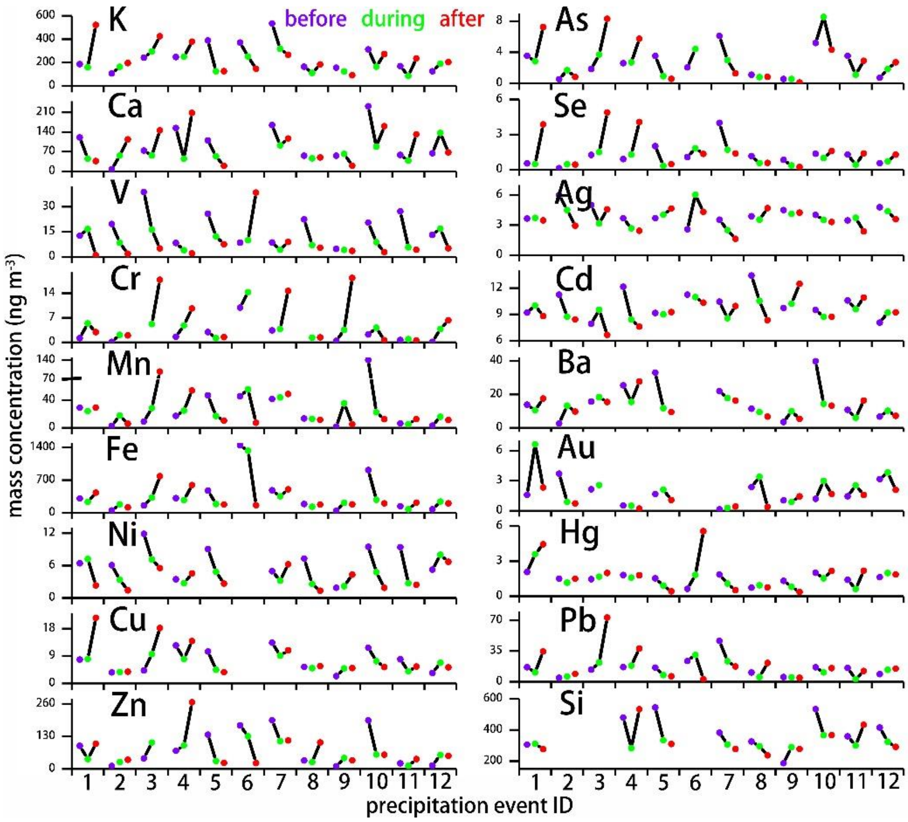

Figure S14. Variation of the mass concentration of each elemental species before, during, and after every precipitation event.